Electronic properties of $GaSe/MoS_2$ and $GaS/MoSe_2$ heterojunctions from first principles calculations

Khang D. Pham, Huynh V. Phuc, Nguyen N. Hieu, Bui D. Hoi, and Chuong V. Nguyen

Citation: AIP Advances **8**, 075207 (2018); doi: 10.1063/1.5033348
View online: https://doi.org/10.1063/1.5033348
View Table of Contents: http://aip.scitation.org/toc/adv/8/7
Published by the American Institute of Physics

AIP | Conference Proceedings

Get 30% off all print proceedings!

Enter Promotion Code PDF30 at checkout

AIP ADVANCES **8**, 075207 (2018)

Electronic properties of $GaSe/MoS_2$ and $GaS/MoSe_2$ heterojunctions from first principles calculations

Khang D. Pham,[1,2,a] Huynh V. Phuc,[3] Nguyen N. Hieu,[4] Bui D. Hoi,[5] and Chuong V. Nguyen[6,b]

[1]*Theoretical Physics Research Group, Advanced Institute of Materials Science, Ton Duc Thang University, Ho Chi Minh City, Viet Nam*
[2]*Faculty of Applied Sciences, Ton Duc Thang University, Ho Chi Minh City, Viet Nam*
[3]*Division of Theoretical Physics, Dong Thap University, Dong Thap, Viet Nam*
[4]*Institute of Research and Development, Duy Tan University, Da Nang, Viet Nam*
[5]*Department of Physics, University of Education, Hue University, Hue, Viet Nam*
[6]*Department of Materials Science and Engineering, Le Quy Don Technical University, Ha Noi, Viet Nam*

(Received 5 April 2018; accepted 26 June 2018; published online 6 July 2018)

In this work, we theoretically investigate electronic properties of $GaSe/MoS_2$ and $GaS/MoSe_2$ heterojunctions using density functional theory based on first-principles calculations. The results show that both $GaSe/MoS_2$ and $GaS/MoSe_2$ heterojunctions are characterized by the weak vdW interactions with a corresponding interlayer distance of 3.45 Å and 3.54 Å, and the binding energy of −0.16 eV per GaSe/GaS cell. Furthermore, one can observe that both the $GaSe/MoS_2$, and $GaS/MoSe_2$ heterojunctions are found to be indirect band gap semiconductors with a corresponding band gap of 1.91 eV and 1.23 eV, respectively. We also find that the band gaps of these semiconductors belong to type II band alignment. A type–II band alignment in both $GaSe/MoS_2$ and $GaS/MoSe_2$ heterojunctions open their potential applications as novel materials such as in designing and fabricating new generation of photovoltaic and optoelectronic devices. © *2018 Author(s). All article content, except where otherwise noted, is licensed under a Creative Commons Attribution (CC BY) license (http://creativecommons.org/licenses/by/4.0/).* https://doi.org/10.1063/1.5033348

I. INTRODUCTION

Graphene, a two-dimensional (2D) monolayer of carbon atoms, is expected to be a promising material for applications in nanotechnology due to its impressive physical properties.[1–3] However, graphene has no band gap, causing a big problem for applications in electronic devices and semiconductor technology.[4] To recovery this point, in parallel with the efforts on changing graphene's properties, an another research field has been intensively gaining in about the past five years that deals with the single-layer post-transition-metal chalcogenides (PTMCs) MX (M = Ga, X = S, Se)[5–9] and transition metal dichalcogenides (TMDs) MY_2 (M = Mo, Y = S, Se),[10–15] and van der Waals (vdW) heterostructures formed by two different single-layer crystals stacking on top of each other.[16–20]

Recently, scientists have successfully synthesized some 2D single-layer PTMCs (GaSe, GaS) and TMDs (MoS_2, $MoSe_2$) that have extraordinary physical properties with prospective applications. *Kim* and co-workers have synthesized a monolayer MoS_2 on the copper substrate by using physical vapor deposition.[21] Also, monolayers MoS_2 and $MoSe_2$ have been synthesized by the liquid exfoliation.[22,23] This can be considered as a motivation for scientists to continue studying these materials. The structural and electronic properties of some TMDs MY_2 have been investigated by first-principles.[13,24–27] Effect of strain and external electric field on the electronic and transport

[a]Electronic mail: phamdinhkhang@tdt.edu.vn
[b]Electronic mail: chuongnguyen11@gmail.com

 © Author(s) 2018

properties of the TMDs has also studied by different methods.[14,28–30] Also, the effect of high pressure on electronic structure and thermoelectric properties of some dichalcogenides has been investigated by first principles calculations.[31,32]

Similar to dichalcogenides, chalcogenides PTMCs (GaSe, GaS) have also attracted much interest of the research community, including theoretical studies.[7–9,33] Researchers showed that electronic, transport and optical properties of those chalcogenides are sensitive to external conditions such as strain or electric field. Currently, numerous nanoelectronic and optoelectronic devices based on GaX crystals such as photodetector,[34] transistors[35] have been successfully fabricated, opening promising potential applications in nanoelectronics and optoelectronics.

In parallel with the efforts on graphene-like materials, the study of heterojunctions by combining two semiconductors has become a hot topic in semiconductor technology.[17,36–40] On the one hand, scientists have successfully investigated the heterojunctions made of graphene and other 2D single-layer semiconductors, such as graphene/h-BN,[41,42] graphene/MoS_2,[43–45] graphene/$MoSe_2$,[46,47] graphene/GaSe.[48–50] On the other hand, they have designed some heterojunctions based on 2D materials, such as PTMC/PTMC,[51,52] TMD/TMD,[53–56] and so on. The studies of these heterojunctions have found many extraordinary properties not occurring in individual materials.

Recently, scientists have paid their attention intensively to some heterojunctions combined of chalcogenides GaX and dichalcogenides MoY_2.[17,18] For example, Zhou and his group[17] for the first time have experimentally synthesized GaSe/MoS_2 heterojunctions by using chemical vapor deposition method and investigated their optoelectronic properties. The results indicate that the GaSe/MoS_2 heterojunctions can be used to open new avenues for the realization of novel 2D nanoelectronic and optoelectronic devices. However, to design and fabricate such devices, it is important to understand the interface properties of those heterojunctions. Moreover, it should be noted that the electronic and transport properties are important properties of materials. If we understand the electronic properties of materials, we can find many ways for application them in real devices, especially electronic devices. To be combined layered-semiconductors, heterojunctions may possess new physical properties are not observed in 2D materials, for example, the appearance of the local energy gap in band structure far from the Fermi level. These new characteristics might open many ways for applications in heterostructure-based optoelectronic devices. Therefore, in this study, we consider systematically the structural and electronic properties of vdW heterostructures formed by the monochalcogenides MoY_2 and chalcogenides GaX by using density functional theory (DFT) method to better understand the physical mechanism in those heterojunctions.

II. COMPUTATIONAL METHOD AND MODEL

In this work, our calculations are performed by using DFT method based on first principles calculations. The DFT method used in this work is implemented in the Quantum Espresso (PWscf) simulation package.[57] To describe the core–valence and the electron exchange–correlation interactions, we use the frozen-core projector augmented wave (PAW)[58] and the generalized gradient approximation (GGA)[59] of Perdew, Burke, and Ernzerhof (PBE) functional,[60] respectively. It is well-known that the traditional DFT methods are unable to describe correctly van der Waals interactions in 2D vdW heterojunctions. Thus, to describe the weak vdW interactions, existing between GaX and MoY_2 monolayers, a semi-empirical DFT–D2 method with the London dispersion corrections[61] is adopted in the present study. The cut–off energy for the plane-wave expansion and the convergence of energy are set to be 500 eV and 10^{-5} eV, respectively. For relaxation process we use $9 \times 9 \times 1$ k point grid, whereas for electronic calculations a $12 \times 12 \times 1$ is used. The atomic structures are relaxed until the forces are smaller than 0.001 eV/Å. To break the interaction between the periodic images of layers in the z direction, we use a large vacuum space of 25 Å.

III. RESULTS AND DISCUSSION

To study the structural and electronic properties of GaSe/MoS_2 and GaS/$MoSe_2$ heterojunctions, it should be noted that these heterojunctions can be created by stacking different 2D crystals on top of each other, layer-by-layer. Thus, it is necessary to investigate firstly the structural and electronic

TABLE I. The lattice constants, bond thicknesses and band gaps of GaX and MoY_2 monolayers.

Materials	a	E_g	h_1	h_2	l_1	l_2
GaSe	3.742	2.46	2.324	4.776	-	-
GaS	3.612	2.57	2.48	4.65	-	-
MoS_2	3.181	1.79	-	-	1.586	3.17
$MoSe_2$	3.278	1.52	-	-	1.664	3.33

properties of separated GaX and MoY_2 monolayers at the equilibrium state and under strain. The relaxed lattice parameters of GaSe, GaS, MoS_2, and $MoSe_2$ monolayers are listed in Table I. After optimizing the atomic structures, the corresponding lattice constants of GaSe, GaS, MoS_2, and $MoSe_2$ monolayers are 3.74 Å, 3.58 Å, 3.16 Å, and 3.29 Å, respectively. These values are in good agreement with previous results.[8,9,14,62] In addition, after relaxation the vertical bond distances of Ga–Ga (h_1), X–X (h_2) in monolayer GaX, and the bond thicknesses of Mo–Y (l_1), Y–Y (l_2) in monolayer MoY_2 are also given in Table I.

Fig. 1 shows the band structures of GaX and MoY_2 monolayers at the equilibrium state after full geometric optimization. It can be seen that GaX monolayers are an indirect semiconductors, whereas MoY_2 monolayers are direct semiconductors. The indirect band gap of GaSe and GaS monolayers are formed between the lowest unoccupied state of conduction band locating on the Γ path and the highest occupied state of valence band lying on the Γ–M path, as shown in Figs. 1(a) and 1(b). Our calculated indirect band gap for GaSe/GaS monolayers is 2.47/2.57 eV. These values are in agreement with previous results.[8,9] The direct band gap of MoY_2 monolayers is formed between the lowest unoccupied state of the conduction band and the highest occupied state of valence band locating at the high symmetry M point, as shown in Figs. 1(c) and 1(d). Our calculated direct band gap for $MoS_2/MoSe_2$ monolayer is 1.79/1.52 eV, respectively, as listed in Table I. These band gaps are consistent with previous theoretical results.[14,62]

We now design and discuss the atomic structures and electronic properties of $GaSe/MoS_2$ and $GaS/MoSe_2$ heterojunctions. It can be seen from Table I that the lattice mismatch between GaSe and MoS_2 monolayers is about 16 %, between GaS and $MoSe_2$ monolayer is about 8 %. Thus to combine the $GaSe/MoS_2$ and $GaS/MoSe_2$ heterojunctions, we use $\sqrt{3} \times \sqrt{3}$ cells of GaX monolayers to match with 2×2 cells of MoY_2 monolayers. The optimized lattice parameters of $GaSe/MoS_2$ and $GaS/MoSe_2$ heterojunctions are 6.48 Å and 6.26 Å, respectively, as shown in Table II. The lattice mismatch between GaX and MoY_2 monolayers in both heterojunctions is less than 2 %. In Fig. 2 we show the relaxed atomic structure of GaX/MoY_2 heterojunctions at the equilibrium state. One can observe that in both heterojunctions, Mo and Y atoms of MoY_2 layers are located below the center of a hexagonal ring formed by the Ga and X atoms of GaX layers. The thicknesses of Ga–Ga, X–X, Mo–Y, and Y–Y atoms and the interlayer distance between GaX and MoY_2 layers are also respectively marked in Fig. 2 by h, l, and d. After fully optimized, our calculated interlayer distances in $GaSe/MoS_2$ and $GaS/MoSe_2$ heterojunctions are 3.45 Å and 3.54 Å, respectively. These interlayer

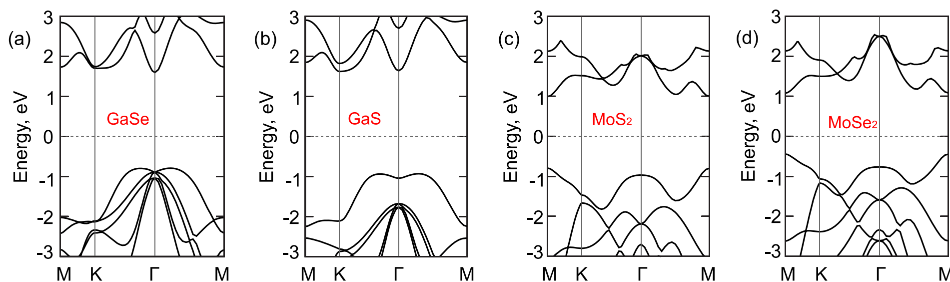

FIG. 1. The electron energy band structures of perfect (a) GaSe, (b) GaS, (c) MoS_2, and (d) $MoSe_2$ monolayers at the equilibrium state, respectively.

TABLE II. The lattice constants, bond thicknesses and band gaps of $GaSe/MoS_2$ and $GaS/MoSe_2$ heterojunctions at the equilibrium state.

Heterostructure	a	E_g	h_1	h_2	d	l_1	l_2
$GaSe/MoS_2$	6.48	1.91	2.43	4.90	3.45	1.58	3.15
$GaS/MoSe_2$	6.26	1.23	2.48	4.72	3.54	1.79	3.58

distances are are in the same order of value with those in other 2D heterojunctions, such as PbI_2/BN,[63] MoS_2/As,[64] $GaS/GaSe$,[51] SnS_2/PbI_2,[65] MoS_2/WS_2,[66] $MoS_2/MoSe_2$[67] heterojunctions.

Furthermore, to evaluate the system stability, we also calculate the binding energy of both $GaSe/MoS_2$ and $GaS/MoSe_2$ heterojunctions. The binding energy of the GaX/MoY_2 can be calculated as follows: $E_b = [E_{GaX/MoY_2} - E_{GaX} - E_{MoY_2}]/n$, where E_{GaX/MoY_2}, E_{GaX}, and E_{MoY_2} are the total energies of combined GaX/MoY_2 heterojunctions, isolated GaX, and MoY_2 monolayers, respectively. n is the number of GaX cells in the heterojunctions, which equals to three. Our calculated binding energies per GaX cell in both $GaSe/MoS_2$ and $GaS/MoSe_2$ heterojunctions are about −0.16 eV. This negative binding energy indicates that both $GaSe/MoS_2$ and $GaS/MoSe_2$ heterojunctions are stable at the equilibrium state. Moreover, we find that the binding energy of GaX/MoY_2 heterojunctions is the same as the binding energy of other 2D vdW heterojunctions, such as SnS_2/PbI_2,[65] MoS_2/WS_2,[66] C_2N/WS_2,[68] P/MoS_2[69] heterojunctions.

We now consider the electronic properties of both $GaSe/MoS_2$ and $GaS/MoSe_2$ heterojunctions. In Fig. 3 we show the electron energy band structure of the $(\sqrt{3} \times \sqrt{3})$ GaSe monolayer, (2×2) MoS_2 monolayer, and the projected $GaSe/MoS_2$ heterojunction. It can be seen that the $(\sqrt{3} \times \sqrt{3})$ GaSe monolayer has a direct band gap of 2.46 eV, formed between the valence band maximum (VBM) and the conduction band minimum (CBM) located at the Γ point, as shown in Fig. 3(a). On the other hand, the (2×2) MoS_2 monolayer has an indirect band gap of about 1.79 eV, that is formed between the VBM locating on the Γ point and the CBM lying on the M–K path, as shown in Fig. 3(b). When the $GaSe/MoS_2$ heterojunction is composed, one can observe that this heterojunction has a type–II staggered gap band alignment with an indirect band gap of 1.91 eV. This indirect band gap is formed by the VBM of GaSe monolayer locating on the Γ–M path and the

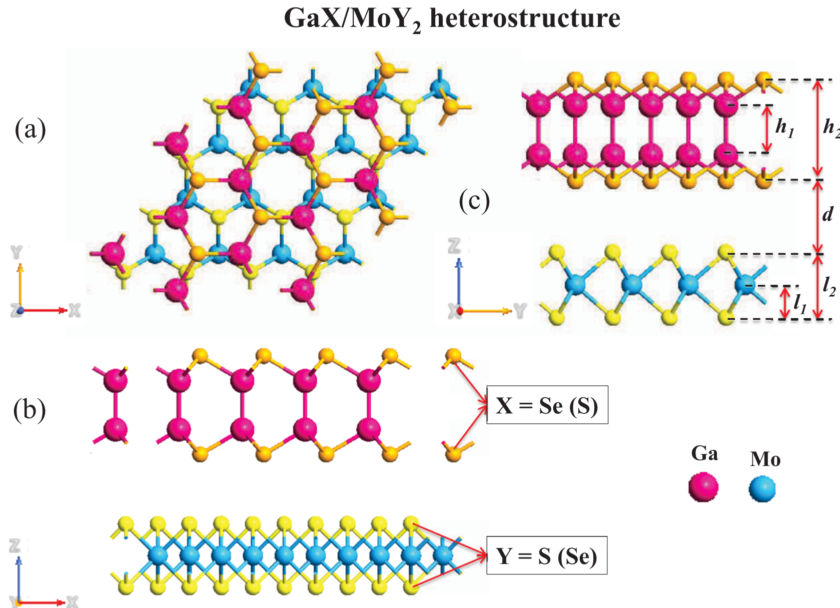

FIG. 2. (a) Top view and (b, c) side views of the atomic structure of GaX/MoY_2 heterojunctions at the equilibrium state. d stands for the interlayer distance between S and Se layers.

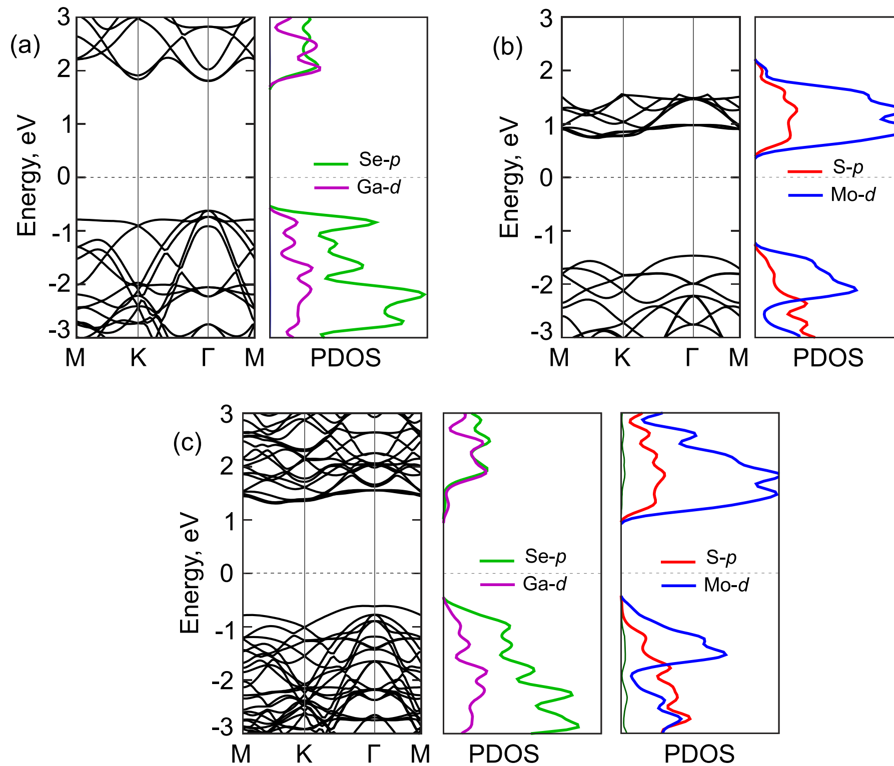

FIG. 3. Calculated band structures and partial density of states (PDOS) of (a) ($\sqrt{3} \times \sqrt{3}$) GaSe monolayer, (b) (2×2) MoS_2 monolayer, and (c) projected $GaSe/MoS_2$ heterojunction, respectively. The Fermi level is set to zero and marked by the dotted line.

CBM of MoS_2 monolayer locating on the M–K path, as shown in Fig. 3(c). It should be noted that a type–II staggered gap band alignment plays an important role in optoelectronic devices, there separate the free holes and electrons spontaneously. Moreover, it can be seen from Fig. 3 that when $GaSe/MoS_2$ heterojunction is composed, the Fermi energy level is shifted downward from the CBM to the VBM of MoS_2 monolayer and shifted upward from the VBM to the CBM of GaSe monolayer.

Similarly, we also calculate the electronic band structures and the projected density of states (PDOS) of ($\sqrt{3} \times \sqrt{3}$) GaS monolayer, (2×2) $MoSe_2$ monolayer, and composed $GaS/MoSe_2$ heterojunction, as shown in Fig. 4. One can observe firstly that the ($\sqrt{3} \times \sqrt{3}$) GaS monolayer is an indirect semiconductor with a band gap of 2.57 eV, forming between the VBM locating on the Γ–K path and the CBM locating on the Γ path, as shown in Fig. 4(a). Also, from Fig. 4(b) we find that (2×2) $MoSe_2$ monolayer has an indirect band gap of 1.52 eV, forming between the CBM located at the K point and VBM locating at the Γ point. By composing the $GaS/MoSe_2$ heterojunction, one can observe that the $GaS/MoSe_2$ heterojunction is a semiconductor with a direct band gap, which is contributed by both the VBM and the CBM appearing at high symmetry Γ point. Our results show that the VBM and CBM are resulted from different GaS and $MoSe_2$ monolayers. As compared to the band structures of GaS and $MoSe_2$ monolayers, the VBM and CBM of $GaS/MoSe_2$ heterojunction are contributed from the VBM of $MoSe_2$ monolayer and the CBM of GaS monolayer, respectively. In this case, the $GaS/MoSe_2$ heterojunction possesses a type–II band alignment. Our calculated direct band gap of $GaS/MoSe_2$ heterojunction is 1.23 eV, which is smaller than that of both GaS and $MoSe_2$ monolayers. This decrease in the band gap of $GaS/MoSe_2$ heterojunction can be understood by analyzing in details the position of the Fermi level, which is shifted upward from the valence band to the conduction band of GaS and $MoSe_2$ monolayers, forming a type–II staggered gap band alignment. A type–II band alignment in both $GaSe/MoS_2$ and $GaS/MoSe_2$ heterojunctions makes their potential applications as novel materials to fabricate and design novel photovoltaic and optoelectronic devices.

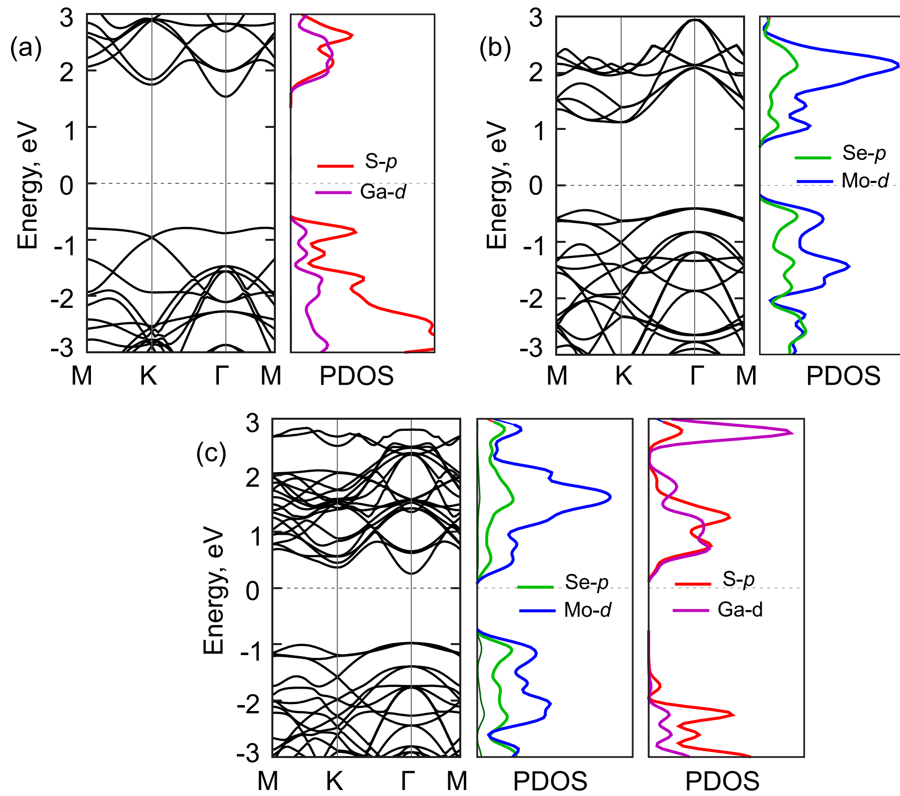

FIG. 4. Calculated band structures and partial density of states (PDOS) of (a) ($\sqrt{3} \times \sqrt{3}$) GaS monolayer, (b) (2 × 2) $MoSe_2$ monolayer, and (c) projected GaS/$MoSe_2$ heterojunction, respectively. The Fermi level is set to zero and marked by the dotted line.

In Fig. 5, we show the electrostatic potential of GaSe/MoS_2 and GaS/$MoSe_2$ heterojunctions at the equilibrium state along the *z* direction. One can observe that the electrostatic potential difference between MoS_2 and GaSe layers is large, in which GaSe monolayer has a deeper potential than that of MoS_2 monolayer. This large potential drop across the GaSe/MoS_2 heterojunction indicates a strong electrostatic field, and may considerably impact the carrier dynamics and charge injection. In contrast, the electrostatic potential of GaS and $MoSe_2$ monolayers is the same. The difference in electrostatic potential indicates the charge transfers from the layer with a higher potential to the layer with a

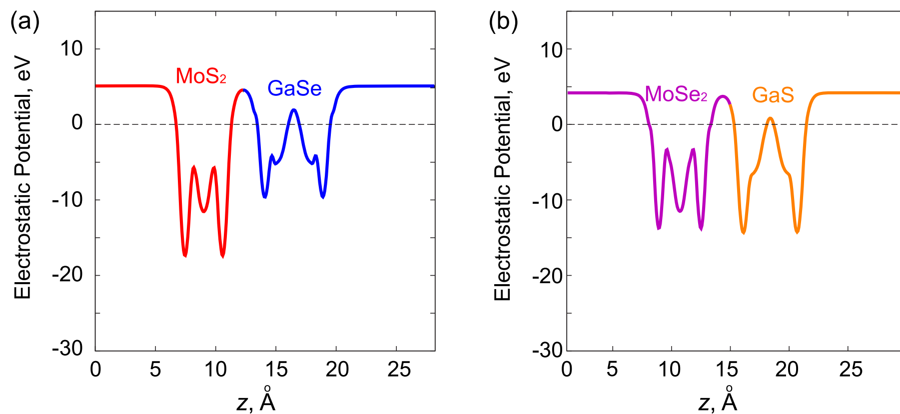

FIG. 5. The electrostatic potential of (a) GaSe/MoS_2 and (b) GaS/$MoSe_2$ heterojunctions at the equilibrium state along the *z* direction.

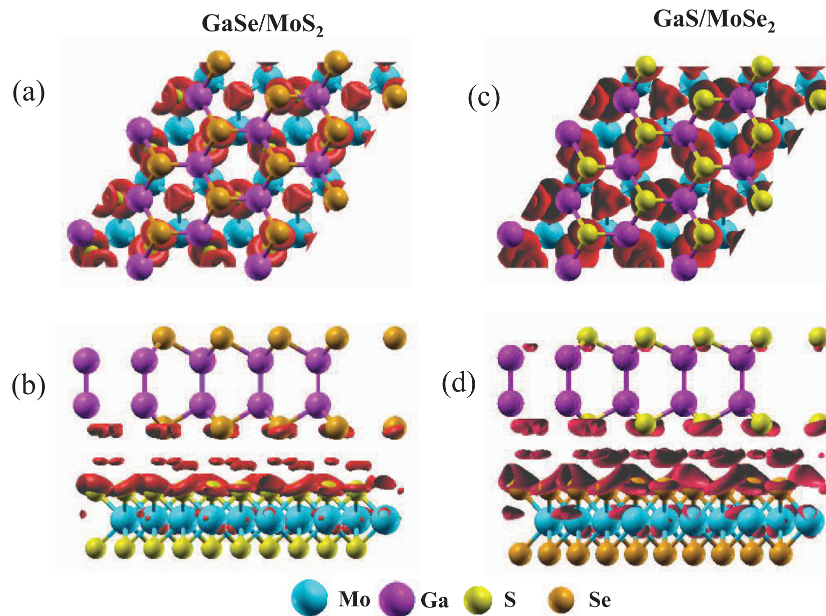

FIG. 6. (a) Top view and (b) side view of the charge density difference in $GaSe/MoS_2$ heterojunction long the z direction. (c) Top view and (d) side view of the charge density difference in $GaS/MoSe_2$ heterojunction along the z direction.

deeper potential. Thus, it is obvious that electrons likely transfer from MoS_2 layer to GaSe layer in the $GaSe/MoS_2$ heterojunction.

For deeper understanding physical mechanism of the charge transfer between GaX and MoY_2 layers in the corresponding GaX/MoY_2 heterojunctions we further consider their charge density difference at the equilibrium state along the z-direction. These results are illustrated in Fig. 6. The charge density difference in the composed heterojunctions is calculated as $\Delta\rho = \rho_{\mathrm{hetero}} - \rho_{\mathrm{GaX}} - \rho_{\mathrm{MoY_2}}$, where ρ_{hetero}, ρ_{GaX}, and $\rho_{\mathrm{MoY_2}}$ are the charge densities of GaX/MoY_2 heterojunctions, GaX monolayer, and MoY_2 monolayer, respectively. One can observe that there are no charge transfer between two GaX and MoY_2 layers. However, we found an evident charge redistribution in the interlayer space of the heterojunctions, as shown in Fig. 6. It can be seen that in both $GaSe/MoS_2$ and $GaS/MoSe_2$ heterojunctions, the charge is accumulated at the topmost S/Se layer of $MoS_2/MoSe_2$ monolayers, and is dissipated at the second Se/S layers of the GaSe/GaS monolayers. It indicates that the charge redistribution is mainly attributes to the electrostatic repulsion.

IV. CONCLUSION

In conclusion, we have investigated systematically the atomic structures and electronic properties of $GaSe/MoS_2$ and $GaS/MoSe_2$ heterojunctions using the density functional theory. The results show that both $GaSe/MoS_2$ and $GaS/MoSe_2$ heterojunctions are characterized by the weak vdW interactions with the corresponding interlayer distance of 3.45 Å and 3.54 Å, respectively and the binding energy of −0.16 eV per GaSe/GaS cell. Furthermore, both $GaSe/MoS_2$, and $GaS/MoSe_2$ heterojunctions are found to be indirect band gap semiconductors with the corresponding band gap of 1.91 eV and 1.23 eV, respectively. We found that these heterojunctions show an indirect band gap with the type-II band alignment. A type–II band alignment in both $GaSe/MoS_2$ and $GaS/MoSe_2$ heterojunctions makes their potential applications as novel materials to fabricate and design novel photovoltaic and optoelectronic devices.

[1] K. S. Novoselov, A. K. Geim, S. V. Morozov, D. Jiang, M. I. Katsnelson, I. V. Grigorieva, S. V. Dubonos, and A. A. Firsov, Nature **438**, 197 (2005).
[2] A. K. Geim and K. S. Novoselov, Nat. Mater. **6**, 183 (2007).
[3] K. S. Novoselov, A. K. Geim, S. V. Morozov, D. Jiang, Y. Zhang, S. V. Dubonos, I. V. Grigorieva, and A. A. Firsov, Science **306**, 666 (2004).
[4] F. Schwierz, Nat. Nanotechnol. **5**, 487 (2010).

[5] Y. Zhou, Y. Nie, Y. Liu, K. Yan, J. Hong, C. Jin, Y. Zhou, J. Yin, Z. Liu, and H. Peng, ACS Nano **8**, 1485 (2014).
[6] X. Li, M.-W. Lin, A. A. Puretzky, J. C. Idrobo, C. Ma, M. Chi, M. Yoon, C. M. Rouleau, I. I. Kravchenko, D. B. Geohegan, and K. Xiao, Sci. Rep. **4**, 5497 (2014).
[7] Y. Ma, Y. Dai, M. Guo, L. Yu, and B. Huang, Physical Chemistry Chemical Physics **15**, 7098 (2013).
[8] L. Huang, Z. Chen, and J. Li, RSC Adv. **5**, 5788 (2015).
[9] M. Yagmurcukardes, R. Senger, F. Peeters, and H. Sahin, Phys. Rev. B **94**, 245407 (2016).
[10] Z. Yin, H. Li, H. Li, L. Jiang, Y. Shi, Y. Sun, G. Lu, Q. Zhang, X. Chen, and H. Zhang, ACS Nano **6**, 74 (2011).
[11] Y.-H. Lee, X.-Q. Zhang, W. Zhang, M.-T. Chang, C.-T. Lin, K.-D. Chang, Y.-C. Yu, J. T.-W. Wang, C.-S. Chang, L.-J. Li *et al.*, Adv. Mater. **24**, 2320 (2012).
[12] M. Kan, J. Wang, X. Li, S. Zhang, Y. Li, Y. Kawazoe, Q. Sun, and P. Jena, J. Phys. Chem. C **118**, 1515 (2014).
[13] R. Roldán, J. A. Silva-Guillén, M. P. López-Sancho, F. Guinea, E. Cappelluti, and P. Ordejón, Annalen der Physik **526**, 347 (2014).
[14] P. Johari and V. B. Shenoy, ACS Nano **6**, 5449 (2012).
[15] H.-P. Komsa and A. V. Krasheninnikov, J. Phys. Chem. Lett. **3**, 3652 (2012).
[16] D. Kong, H. Wang, J. J. Cha, M. Pasta, K. J. Koski, J. Yao, and Y. Cui, Nano Lett. **13**, 1341 (2013).
[17] N. Zhou, R. Wang, X. Zhou, H. Song, X. Xiong, Y. Ding, J. Lü, L. Gan, and T. Zhai, Small, 1702731 (2018).
[18] X. Li, M.-W. Lin, J. Lin, B. Huang, A. A. Puretzky, C. Ma, K. Wang, W. Zhou, S. T. Pantelides, M. Chi, I. Kravchenko, J. Fowlkes, C. M. Rouleau, D. B. Geohegan, and K. Xiao, Sci. Adv. **2**, e1501882 (2016).
[19] C.-x. Xia, J. Du, X.-w. Huang, W.-b. Xiao, W.-q. Xiong, T.-x. Wang, Z.-m. Wei, Y. Jia, J.-j. Shi, and J.-b. Li, Phys. Rev. B **97**, 115416 (2018).
[20] C. V. Nguyen, N. N. Hieu, N. A. Poklonski, V. V. Ilyasov, L. Dinh, T. C. Phong, L. V. Tung, and H. V. Phuc, Phys. Rev. B **96**, 125411 (2017).
[21] D. Kim, D. Sun, W. Lu, Z. Cheng, Y. Zhu, D. Le, T. S. Rahman, and L. Bartels, Langmuir **27**, 11650 (2011).
[22] J. N. Coleman, M. Lotya, A. ONeill, S. D. Bergin, P. J. King, U. Khan, K. Young, A. Gaucher, S. De, R. J. Smith *et al.*, Science **331**, 568 (2011).
[23] R. Ganatra and Q. Zhang, ACS Nano **8**, 4074 (2014).
[24] S. Lebegue and O. Eriksson, Phys. Rev. B **79**, 115409 (2009).
[25] Y. Jing, X. Tan, Z. Zhou, and P. Shen, J. Mater. Chem. A **2**, 16892 (2014).
[26] Y. Li, Z. Zhou, S. Zhang, and Z. Chen, J. Am. Chem. Soc. **130**, 16739 (2008).
[27] Q. Tang, Z. Zhou, and Z. Chen, Wiley Interdiscip. Rev. Comput. Mol. Sci. **5**, 360 (2015).
[28] C. Ataca, M. Topsakal, E. Akturk, and S. Ciraci, J. Phys. Chem. C **115**, 16354 (2011).
[29] H. V. Phuc, N. N. Hieu, B. D. Hoi, N. V. Hieu, T. V. Thu, N. M. Hung, V. V. Ilyasov, N. A. Poklonski, and C. V. Nguyen, J. Electron. Mater. **47**, 730 (2018).
[30] C. V. Nguyen and N. N. Hieu, Chem. Phys. **468**, 9 (2016).
[31] O. Kohulák and R. Martoňák, Phys. Rev. B **95**, 054105 (2017).
[32] H. Guo, T. Yang, P. Tao, Y. Wang, and Z. Zhang, J. Appl. Phys. **113**, 013709 (2013).
[33] T. Cao, Z. Li, and S. G. Louie, Phys. Rev. Lett. **114**, 236602 (2015).
[34] P. Hu, Z. Wen, L. Wang, P. Tan, and K. Xiao, ACS Nano **6**, 5988 (2012).
[35] D. J. Late, B. Liu, J. Luo, A. Yan, H. Matte, M. Grayson, C. Rao, and V. P. Dravid, Adv. Mater. **24**, 3549 (2012).
[36] X. Wang and F. Xia, Nat. Mater. **14**, 264 (2015).
[37] K. S. Novoselov, A. Mishchenko, A. Carvalho, and A. H. Castro Neto, Science **353** (2016).
[38] A. K. Geim and I. V. Grigorieva, Nature **499**, 419 (2013).
[39] B. V. Lotsch, Annual Review of Materials Research **45**, 85 (2015).
[40] M.-Y. Li, C.-H. Chen, Y. Shi, and L.-J. Li, Mater. Today **19**, 322 (2016).
[41] C. R. Dean, A. F. Young, I. Meric, C. Lee, L. Wang, S. Sorgenfrei, K. Watanabe, T. Taniguchi, P. Kim, K. L. Shepard *et al.*, Nat. Nanotechnol. **5**, 722 (2010).
[42] A. V. Lebedev, I. V. Lebedeva, A. M. Popov, and A. A. Knizhnik, Phys. Rev. B **96**, 085432 (2017).
[43] C. V. Nguyen, Superlattices and Microstruct. **116**, 79 (2018).
[44] L. Yu, Y.-H. Lee, X. Ling, E. J. Santos, Y. C. Shin, Y. Lin, M. Dubey, E. Kaxiras, J. Kong, H. Wang *et al.*, Nano Lett. **14**, 3055 (2014).
[45] Y. Ma, Y. Dai, M. Guo, C. Niu, and B. Huang, Nanoscale **3**, 3883 (2011).
[46] Y. Sata, R. Moriya, S. Morikawa, N. Yabuki, S. Masubuchi, and T. Machida, Appl. Phys. Lett. **107**, 023109 (2015).
[47] Y. Ma, Y. Dai, W. Wei, C. Niu, L. Yu, and B. Huang, J. Phys. Chem. C **115**, 20237 (2011).
[48] W. Kim, C. Li, F. A. Chaves, D. Jiménez, R. D. Rodriguez, J. Susoma, M. A. Fenner, H. Lipsanen, and J. Riikonen, Adv. Mater. **28**, 1845 (2016).
[49] C. Si, Z. Lin, J. Zhou, and Z. Sun, 2D Materials **4**, 015027 (2016).
[50] Z. Ben Aziza, H. Henck, D. Pierucci, M. G. Silly, E. Lhuillier, G. Patriarche, F. Sirotti, M. Eddrief, and A. Ouerghi, ACS Nano **10**, 9679 (2016).
[51] W. Wei, Y. Dai, C. Niu, X. Li, Y. Ma, and B. Huang, J. Mater. Chem. C **3**, 11548 (2015).
[52] X.-B. Chen and D. F. Kelley, J. Phys. Chem. B **110**, 25259 (2006).
[53] B. Amin, T. P. Kaloni, G. Schreckenbach, and M. S. Freund, Appl. Phys. Lett. **108**, 063105 (2016).
[54] J. Kang, J. Li, S.-S. Li, J.-B. Xia, and L.-W. Wang, Nano Lett. **13**, 5485 (2013).
[55] Q. Wang, P. Wu, G. Cao, and M. Huang, J. Phys. D Appl. Phys. **46**, 505308 (2013).
[56] B. Amin, N. Singh, and U. Schwingenschlögl, Phys. Rev. B **92**, 075439 (2015).
[57] P. Giannozzi, S. Baroni, N. Bonini, M. Calandra, R. Car, C. Cavazzoni, D. Ceresoli, G. L. Chiarotti, M. Cococcioni, I. Dabo, A. D. Corso, S. de Gironcoli, S. Fabris, G. Fratesi, R. Gebauer, U. Gerstmann, C. Gougoussis, A. Kokalj, M. Lazzeri, L. Martin-Samos, N. Marzari, F. Mauri, R. Mazzarello, S. Paolini, A. Pasquarello, L. Paulatto, C. Sbraccia, S. Scandolo, G. Sclauzero, A. P. Seitsonen, A. Smogunov, P. Umari, and R. M. Wentzcovitch, J. Phys. Conden. Matter **21**, 395502 (2009).

[58] P. E. Blöchl, Phys. Rev. B **50**, 17953 (1994).
[59] J. P. Perdew, K. Burke, and M. Ernzerhof, Phys. Rev. Lett. **77**, 3865 (1996).
[60] J. Perdew, K. Burke, and M. Ernzerhof, Phys. Rev. Lett. **80**, 891 (1998).
[61] S. Grimme, Wiley Interdiscip. Rev. Comput. Mol. Sci. **1**, 211 (2011).
[62] A. Ramasubramaniam, Phys. Rev. B **86**, 115409 (2012).
[63] Y. Ma, X. Zhao, M. Niu, X. Dai, W. Li, X. Wang, M. Zhao, T. Wang, and Y. Tang, Appl. Surf. Sci. **411**, 46 (2017).
[64] W. Li, T. Wang, X. Dai, Y. Ma, and Y. Tang, J. Alloys Compd. **705**, 486 (2017).
[65] Y. Ma, X. Zhao, M. Niu, X. Dai, W. Li, Y. Li, M. Zhao, T. Wang, and Y. Tang, RSC Adv. **7**, 25582 (2017).
[66] K. Kośmider and J. Fernández-Rossier, Phys. Rev. B **87**, 075451 (2013).
[67] F. Ceballos, M. Z. Bellus, H.-Y. Chiu, and H. Zhao, ACS Nano **8**, 12717 (2014).
[68] R. Kumar, D. Das, and A. K. Singh, J. Catal. **359**, 143 (2018).
[69] L. Huang, N. Huo, Y. Li, H. Chen, J. Yang, Z. Wei, J. Li, and S.-S. Li, J. Phys. Chem. Lett. **6**, 2483 (2015).